Nonparabolic coupled Poisson-Schrödinger solutions for quantized electron accumulation layers: Band bending, charge profile, and subbands at InN surfaces

P. D. C. King, T. D. Veal, and C. F. McConville*
Department of Physics, University of Warwick, Coventry CV4 7AL, United Kingdom
(Received 20 November 2007; published 5 March 2008)

The one-electron potential, carrier concentration profile, quantized subband state energies, and parallel dispersion relations are calculated for an accumulation layer at a semiconductor surface by solving Poisson's equation within a modified Thomas-Fermi approximation and numerically solving the Schrödinger equation for the resulting potential well. A nonparabolic conduction band, described within the Kane $\mathbf{k}\cdot\mathbf{p}$ approximation, is incorporated in the model. Example calculations are performed for a typical clean InN surface and for a variety of surface state densities and bulk carrier concentrations. Agreement is found between the model calculations and experimental measurements of the subband energies and dispersions at *c*-plane InN surfaces from electron tunneling spectroscopy and angle resolved photoemission spectroscopy.

DOI: 10.1103/PhysRevB.77.125305 PACS number(s): 73.20.−r, 73.61.Ey, 79.60.−i

I. INTRODUCTION

At a surface or interface of a semiconductor, the breaking of the translational symmetry of the crystal allows evanescent gap states to exist within the semiconductor band gap. These have either donor or acceptor character, largely dependent on their position relative to the charge neutrality level (CNL) of the semiconductor.[1] Charged surface (interface) states induce an electric field, which is screened by a rearrangement of the carriers in the near-surface (interface) region, over a distance approximately equal to the Thomas-Fermi screening length, leading to regions of carrier depletion or accumulation close to the surface (interface).

A surface accumulation of electrons can be generated by applying a bias, for example, in a metal-oxide-semiconductor (MOS) system. However, it is of special interest where the accumulation is an inherent property of the material. If unoccupied, and hence positively charged, donor surface states are present, the bands will bend downward relative to the Fermi level leading to an accumulation of electrons at the surface. Such an intrinsic accumulation of electrons has been observed at the clean surface of both InAs (Ref. 2) and InN,[3] with significantly higher surface state densities observed in the latter material.

If the downward band bending associated with the electron accumulation (or inversion for *p*-type material) is sufficiently deep and narrow, the potential well created at the surface causes the conduction band states normal to the surface to become quantized into a number of discrete levels.[4] This effect was first experimentally observed in Si MOS structures by magnetoresistance measurements[5] confirmed by far-infrared intersubband optical absorption.[6] Quantized states have also been observed in intrinsic accumulation layers by Tsui[7–9] and Veal *et al.*[10,11] who employed electron tunneling spectroscopy to observe quantized levels at the surface of InAs and InN and In-rich InGaN, respectively. As the downward band bending is in the direction normal to the surface, the quantization is in this direction only; consequently, the motion of carriers in the plane of the surface remains free, and the subbands that form are two dimensional. The dispersion of these subbands has been directly observed by angle resolved photoemission spectroscopy (ARPES) at InAs (Ref. 12) and InN (Ref. 13) surfaces.

The effective one-electron potential at a semiconductor surface, and corresponding variation in carrier density, is strictly described by a self-consistent solution of the Poisson and Schrödinger equations.[14] As the solution of the Schrödinger equation is dependent on the potential derived from a solution of Poisson's equation, this procedure is highly nonlinear. Several methods have been previously employed to assist convergence of the self-consistent iteration. Baraff and Appelbaum[14] and Ehlers and Mills[15] performed self-consistent Poisson-Schrödinger (PS) Hartree calculations employing a parametrized Morse potential, which allows a series solution of the Schrödinger equation to be made, without the need for full numerical solutions. Streight and Mills[16] employed a Fourier and a finite-difference method to determine self-consistent PS Hartree solutions for an electrically neutral finite semiconductor slab. The finite geometry of the slab makes achieving self-consistency easier, although the solutions do not necessarily apply to semi-infinite systems. The above schemes also assumed parabolic dispersion of the semiconductor bands.

Inaoka[17] employed a local-density-approximation (LDA) calculation within a semiconductor slab thick enough to ensure that the potential and carrier distribution at the surface of the slab is equivalent to that for the semi-infinite system. Nonparabolicity of the conduction band was approximately included by a modification of the effective mass to that at the Fermi level for a nonparabolic (NP) dispersion. This approach was subsequently extended to include the full conduction band nonparabolicity in the self-consistent PS LDA solutions.[18] The incorporation of nonparabolicity, however, makes these calculations very computationally intensive.

An alternative approach to full self-consistent PS solutions is to solve Poisson's equation within a modified Thomas-Fermi approximation (MTFA), developed for parabolic bands by Paasch and Übensee.[19] Within the MTFA, an infinite potential step is assumed at the surface, and the local density of states is modified to approximate the effects of quantum-mechanical reflection at this barrier. This method has subsequently been extended to incorporate a NP conduc-

tion band.[20] The MTFA approximation has been shown to be in excellent agreement with full self-consistent PS solutions for parabolic conduction band dispersions.[19,21] However, although this method generates very similar one-electron potentials and charge profiles to self-consistent PS solutions, it does not contain any information on the subband structure present when strong band bending at the semiconductor surface causes the conduction band states to become quantized.

This paper presents details of a method combining the Poisson-MTFA solution with a numerical solution of the Schrödinger equation for the resulting one-electron potential to yield the conduction subband structure. Section II introduces the theoretical constructs used in the model. The calculations can be performed with relatively little computational cost, and these are shown to yield results in good agreement with full self-consistent NP PS solutions. Section III contains example results for accumulation layers at InN surfaces. Finally, in Sec. IV, the method of calculation is successfully used to simulate recently observed[10,13] experimental measurements of subbands at InN surfaces.

II. THEORY

A. Band structure approximations

It is important to include the nonparabolicity of the conduction band within the calculations. A simple form of the NP conduction band dispersion can be obtained using Kane's $\mathbf{k}\cdot\mathbf{p}$ formalism,[22] described by the Hamiltonian

$$\mathcal{H} = \begin{bmatrix} \tilde{\mathcal{H}} & 0 \\ 0 & \tilde{\mathcal{H}} \end{bmatrix}, \tag{1a}$$

where

$$\tilde{\mathcal{H}} = \begin{bmatrix} E_s & 0 & kP & 0 \\ 0 & E_p - \Delta_{so}/3 & \sqrt{2}\Delta_{so}/3 & 0 \\ kP & \sqrt{2}\Delta_{so}/3 & E_p & 0 \\ 0 & 0 & 0 & E_p + \Delta_{so}/3 \end{bmatrix}, \tag{1b}$$

where E_s (E_p) is the conduction (valence) band edge energy, Δ_{so} is the spin-orbit splitting, k is the wave vector, and P is Kane's matrix element. The material is assumed to be isotropic and have no crystal field splitting. For InN, the crystal field splitting is small,[23] and only a small anisotropy in the effective mass has been observed,[24] indicating that the conduction band dispersion is adequately described under these assumptions. The conduction band dispersion is described by

$$E_c(k) = E' + E_k, \tag{2}$$

where

$$E_k = \frac{\hbar^2 k^2}{2m_0}, \tag{3}$$

where m_0 is the free electron mass and E' is the largest eigenvalue of the Hamiltonian [Eqs. (1a) and (1b)] given by the largest solution of the algebraic equation

$$E'(E' + E_g)(E' + E_g + \Delta_{so}) - k^2P^2(E' + E_g + 2\Delta_{so}/3) = 0, \tag{4}$$

where $E_s=0$ and $E_p=-E_g-\Delta_{so}/3$ have been used, defining the zero of energy at the conduction band minimum (CBM). Kane's matrix element is given by

$$P^2 = \frac{3\hbar^2(1/m_0^* - 1/m_0)}{2[2/E_g + 1/(E_g + \Delta_{so})]}, \tag{5}$$

where m_0^* is the conduction band edge effective mass.

A useful simplifying approximation, applicable in InN where $\Delta_{so} \ll E_g$,[23] is to neglect the spin-orbit splitting. In this case, solving Eq. (4) gives the familiar two-band $\mathbf{k}\cdot\mathbf{p}$ analytic form for the conduction band dispersion

$$E_c(k) = \frac{1}{2}[-E_g + \sqrt{E_g^2 + 4k^2P^2}] + E_k, \tag{6}$$

Kane's matrix element simplifies to

$$P^2 = \frac{\hbar^2}{2m_0}\left(\frac{m_0}{m_0^*} - 1\right)E_g, \tag{7}$$

and the density of conduction band states is given by

$$g_c(k) = \frac{k^2}{\pi^2}\left[\frac{dE_c(k)}{dk}\right]^{-1} = \frac{k/\pi^2}{4P^2[E_g^2 + 4k^2P^2]^{-1/2} + (\hbar^2/m_0)}. \tag{8}$$

B. Poisson–MTFA formalism

The one-electron potential $V(z)$, describing the band bending in the space-charge region as a function of depth z below a semiconductor surface, must satisfy Poisson's equation[25]

$$\frac{d^2V}{dz^2} = -\frac{e}{\varepsilon(0)\varepsilon_0}[N_D^+ - N_A^- - n(z) + p(z)], \tag{9}$$

where $\varepsilon(0)$ is the static dielectric constant, N_D^+ (N_A^-) is the bulk donor (acceptor) density, assumed constant throughout the semiconductor, and $n(z)$ [$p(z)$] is the electron (hole) density. The potential $V(z)$ must satisfy the boundary conditions

$$V(z) \to 0 \quad \text{as } z \to \infty, \tag{10a}$$

as charge neutrality requires that there can be no band bending in the bulk of the semiconductor and

$$\left.\frac{dV}{dz}\right|_{z=0} = \frac{e}{\varepsilon(0)\varepsilon_0}N_{ss}, \tag{10b}$$

where N_{ss} is the surface state density. Alternatively, it is equivalent to consider the total band bending at the surface as a boundary condition.

Within the MTFA,[19] the potential is calculated by solving the Poisson equation subject to the boundary conditions [Eqs. (10a) and (10b)] with the carrier densities corresponding to the conduction and valence bands calculated, respectively, from

$$n(z) = \int_0^{\infty} g_c(E) f_{FD}(E) f(z) dE, \tag{11a}$$

$$p(z) = \sum_i \int_{E_{V_i}}^{-\infty} g_{v_i}(E)[1 - f_{FD}(E)] f(z) dE, \tag{11b}$$

where the sum over i denotes the sum over a number of valence bands, $g_c(E)$ $[g_{v_i}(E)]$ is the density of states for the NP conduction [ith valence] band, f_{FD} is the Fermi-Dirac function including the potential dependence

$$f_{FD}(E) = \frac{1}{1 + \exp\{\beta[E - E_F + V(z)]\}}, \tag{12}$$

where E_F is the Fermi energy and $\beta = \frac{1}{k_B T}$, and $f(z)$ is the MTFA factor to account for the potential barrier at the surface,[20]

$$f(z) = 1 - \mathrm{sinc}\left[\frac{2z}{L}\left(\frac{E}{k_B T}\right)^{1/2}\left(1 + \frac{E}{E_g}\right)^{1/2}\right], \tag{13}$$

where, for nondegenerate semiconductors, L is the thermal length $L = \hbar/(2m_0^* k_B T)^{1/2}$ and, for degenerate semiconductors, $L = \frac{1}{k_F}$ is the Fermi length. Physically, this correction factor $f(z)$ represents the interference of incident and reflected wave functions due to the potential barrier at the surface. As the characteristic penetration length of the wave functions into the vacuum is very short, much shorter than the variation of carrier density in the space-charge region, it is a good approximation to impose the boundary condition that the wave function is equal to zero at the surface and thus that the carrier concentration tends smoothly to zero at the surface; this is ensured by the MTFA correction. The integral limit E_{V_i} in Eq. (11b) denotes the valence band maximum (VBM) of the ith valence band allowing for spin-orbit and crystal field splittings.

Numerical solution of Eqs. (9), (11a), and (11b) is initialized using a trial potential; an interval bisection method is then employed to converge to a solution of the one-electron (band bending) potential that satisfies the boundary conditions [Eqs. (10a) and (10b)]. For accumulation and depletion layers, the minority carrier concentration can, without loss of information, generally be assumed to be zero in the calculations.

C. Schrödinger equation solution

The numerical solution of the Schrödinger equation for the one-electron potential determined by the solution of the Poisson-MTFA calculations proceeds via a Fourier-series representation.[16,18] The one-electron (band bending) potential destroys the translational symmetry of the crystal. It is therefore appropriate to express the Schrödinger equation in terms of envelope functions made up of Wannier functions $\Psi(\mathbf{r}_\parallel, z)$, where $\mathbf{r}_\parallel$ (z) is the parallel (normal) component of the position vector. In this representation, the Schrödinger equation is given by[18,26]

$$[E_c(-i\nabla) + V(z)]\Psi(\mathbf{r}_\parallel, z) = E\Psi(\mathbf{r}_\parallel, z), \tag{14}$$

where the eigenfunction for a subband j and a given parallel wave vector $\mathbf{k}_\parallel$ is

$$\Psi_{\mathbf{k}_\parallel, j}(\mathbf{r}_\parallel, z) = \frac{1}{\sqrt{A}} \exp(i\mathbf{k}_\parallel \cdot \mathbf{r}_\parallel) \psi_{\mathbf{k}_\parallel, j}(z), \tag{15}$$

where A is a normalization factor and $\psi_{\mathbf{k}_\parallel, j}(z)$ is the component of the eigenfunction normal to the surface for a given subband and parallel wave vector.

Imposing the boundary condition (as above) that the wave functions vanish at the surface $(z=0)$ and assuming a system of some length ℓ, such that the wave functions have also decayed to zero by $z=\ell$, $\psi_{\mathbf{k}_\parallel, j}(z)$ can be expanded as a Fourier sine series

$$\psi_{\mathbf{k}_\parallel, j}(z) = \sum_{\nu=1}^{\infty} \sqrt{\frac{2}{\ell}} a_\nu^{\mathbf{k}_\parallel, j} \sin\left(\frac{\nu\pi}{\ell} z\right). \tag{16}$$

Substituting this into the Schrödinger equation [Eq. (14)] gives the matrix representation of the problem for a given $\mathbf{k}_\parallel$,

$$\mathbf{M}^{\mathbf{k}_\parallel} \mathbf{a}^{\mathbf{k}_\parallel} = E^{\mathbf{k}_\parallel} \mathbf{a}^{\mathbf{k}_\parallel}, \tag{17a}$$

where the matrix elements are given by

$$[\mathbf{M}]_{\nu\nu'} = E_c(k_\nu)\delta_{\nu\nu'} + \frac{2}{\ell}\int_0^{\ell} dz V(z) \sin\left(\frac{\nu\pi}{\ell} z\right)\sin\left(\frac{\nu'\pi}{\ell} z\right), \tag{17b}$$

where $k_\nu = \sqrt{\mathbf{k}_\parallel^2 + (\nu\pi/\ell)^2}$ and $\delta_{\nu\nu'}$ is the Kronecker delta function. The eigenvalues and eigenfunctions of $\mathbf{M}$ can therefore be used to determine the confined subband energies and wave functions normal to the surface for a given one-electron potential calculated from the Poisson-MTFA solution. In practice, the infinite sum in Eq. (16) is truncated after an order ν_{max}, giving a $\nu_{max} \times \nu_{max}$ matrix in Eqs. (17a) and (17b). The value of ν_{max} required to ensure convergence of the eigenvalues is dependent on the depth and width of the surface potential well. Setting $\nu_{max} = 500$ was found to be sufficient for all cases considered here.

D. Verification of model

Calculation of properties of the accumulation layer proceeds as follows. First, the one-electron potential $V(z)$ and depth-dependent carrier concentration $n(z)$ are calculated by the solution of Poisson's equation within the MTFA approximation (Sec. II B) incorporating a NP conduction band dispersion (Sec. II A). The Schrödinger equation is then solved numerically for the resulting potential (Sec. II C) incorporating the same NP conduction band dispersion to yield subband energies and parallel dispersions. In this method, the Schrödinger equation has only to be solved numerically once for each value of the parallel wave vector (due to the conduction band nonparabolicity) for the one-electron potential calculated from the Poisson-MTFA formalism. This is in contrast to full self-consistent NP solutions where the Schrödinger equation has to be solved numerically (for each parallel wave vector) for multiple one-electron potentials in

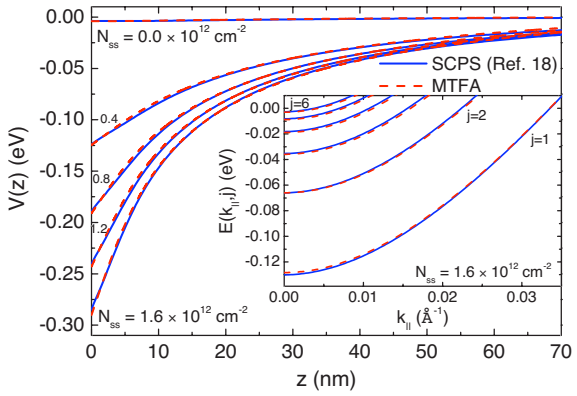

FIG. 1. (Color online) The one-electron potential $V(z)$ as a function of depth below the surface, z, for InAs, using the material parameters in Table I. Self-consistent Poisson-Schrödinger (SCPS) calculations (solid lines, Ref. 18) and Poisson-MTFA calculations (dashed lines, this work) are shown for surface sheet densities of $N_{ss}=0.0\times10^{12}$, 0.4×10^{12}, 0.8×10^{12}, 1.2×10^{12}, and 1.6×10^{12} cm^{-2} and a bulk carrier density of $n=1.3\times10^{16}$ cm^{-3}. For a surface sheet density of $N_{ss}=1.6\times10^{12}$, the calculated (SCPS and MTFA-Schrödinger approximation) subband dispersions are shown, inset.

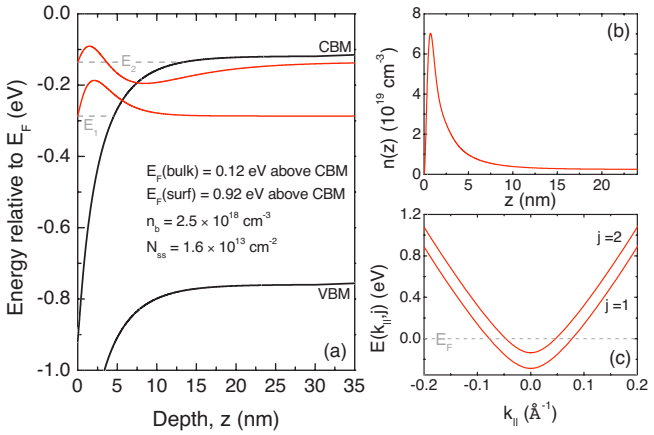

FIG. 2. (Color online) (a) Downward band bending at an InN surface with a surface sheet density of $N_{ss}=1.6\times10^{13}$ cm^{-2} and bulk carrier density of $n_b=2.5\times10^{18}$ cm^{-3} and (b) corresponding near-surface carrier density. Two quantized states form (E_1 and E_2) and their corresponding (a) wave functions and (c) parallel dispersion relations are shown.

order to iteratively proceed toward a self-consistent solution, therefore proving significantly more computationally intensive than the coupled method presented here.

To verify the model, the one-electron potential for a variety of surface state densities and a set of subband dispersions calculated by this model for InAs surfaces are compared to the full self-consistent NP PS calculations of Abe *et al.*[18] in Fig. 1. The InAs parameters used are listed in Table I. The one-electron potentials and subband dispersions agree very well between the two calculation methods, confirming the validity of the NP coupled Poisson-MTFA/Schrödinger method as a good approximation to full self-consistent NP PS calculations. The calculations presented in the remainder of the paper are for higher surface state densities than those calculated by Abe *et al.*,[18] as compared to here. However, the comparison of the one-electron potentials shown in Fig. 1 does not show signs of increased deviation as the surface state density is increased by over an order of magnitude. The agreement between the self-consistent NP PS calculations and the calculations presented here is therefore expected to hold for the higher surface state densities used in the remainder of this work.

TABLE I. Material parameters [band gap (E_g) and Varshni parameters (α,β), band edge effective mass (m_0^*), and spin-orbit splitting (Δ_{so})] for InAs and InN.

	InAs[a]	InN
E_g (eV)	0.3543[b]	0.690[c]
α (meV/K)		0.41[c]
β (K)		454[c]
m_0^* (m_0)	0.02195	0.048[d]
Δ_{so} (eV)	0.381	0

[a]The InAs parameters are those employed by Abe *et al.* (Ref. 18) in their calculations.
[b]At 295 K.
[c]Zero temperature band gap and Varshni parameters from Ref. 27.
[d]Zero temperature value based on the empirical relationship $m_e^*\sim0.07E_g$ (Ref. 28) which is very close to the value of $0.047m_0$ determined by Hofmann *et al.* (Ref. 24) from infrared magneto-optic generalized ellipsometry.

III. InN ACCUMULATION LAYERS

For moderately doped InN, a pronounced universality of the electron accumulation has been observed at the clean surface of both polar and nonpolar InN,[29] with typical surface state densities of $\sim1.6\times10^{13}$ cm^{-2}. The simulated results of such a typical accumulation layer in InN, using the material parameters in Table I with a surface sheet density $N_{ss}=1.6\times10^{13}$ cm^{-2} and bulk carrier density $n_b=2.5\times10^{18}$ cm^{-3}, are shown in Fig. 2. Donor surface states pin the surface Fermi level close to, but slightly below, the CNL in InN. Due to the low Γ-point CBM in InN, the CNL lies significantly above the band edges in this material[30] ($\sim$1.8 eV above the VBM[31]). Consequently, the Fermi level is pinned far above the CBM at the surface. Donor surface states above the CBM donate their electrons directly into the conduction band, leading to a large accumulation of electrons and an extreme downward bending of the bands relative to the Fermi level at the surface. This forms a deep potential well at the surface where the conduction band states become quantized.

Two such quantized states are obtained for the current example. The normal components of the eigenfunctions are shown superimposed on the subbands in Fig. 2(a). The wave functions are equal to zero at the surface ($z=0$) due to the imposed boundary condition here. Also, the wave functions decay into the potential barrier, such that a long way from the surface, they have zero amplitude. It is the peak of these wave functions close to the surface that is responsible for the

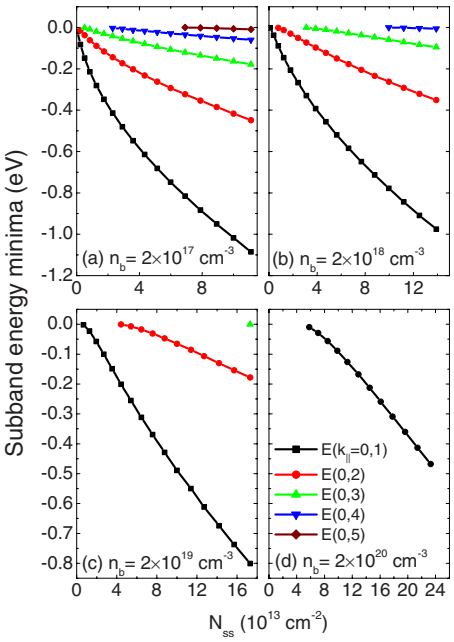

FIG. 3. (Color online) Variation in energy of the subband minima relative to the bulk CBM (top of the potential well) with surface state density for bulk carrier concentrations of (a) 2×10^{17} cm^{-3}, (b) 2×10^{18} cm^{-3}, (c) 2×10^{19} cm^{-3}, and (d) 2×10^{20} cm^{-3}. The points show the calculated subband energy minima for a downward band bending (right to left) of 3.3, 3.1, 2.9, 2.7,…, eV.

peak in the carrier concentration in the accumulation layer [Fig. 2(b)].

The parallel dispersion of the subbands is also obtained from the model [Fig. 2(c)]. These dispersions become rather linear with increasing $k_{\|}$, indicating a distinct nonparabolicity. However, this nonparabolicity is not simply described by a Kane-like dispersion, instead, requiring the full numerical solution of the Schrödinger equation for different values of $k_{\|}$.

Although the Fermi level is strongly pinned at clean InN surfaces, it is possible to induce changes in the pinning position in a number of ways. A large increase in the bulk doping level has been observed to increase the Fermi level pinning position, in order to maintain charge neutrality.[31] The changes in the measured conductivity of InN when exposed to a number of solvents and gases have been attributed to changes in the surface electronic properties.[32,33] Additionally, the deposition on the surface of metals of varying electronegativity can cause a variation in the Fermi level pinning position.[1] For example, the deposition of small amounts of Cs on InAs(110) surfaces has been shown[34] to lead to a large enhancement of the electron accumulation. The variation in surface state density and corresponding downward band bending associated with these modifications to the clean surface will cause a pronounced variation in the number and confinement energies of the subbands. This is represented by the variation in subband energy minima for a variety of surface state densities and bulk carrier densities shown in Fig. 3.

With increasing surface state density, the amount of downward band bending increases, and so the potential well becomes deeper at the surface. This causes the number of subbands bound within the well to increase and the subbands to become confined deeper within the well. Conversely, with increasing bulk doping, fewer subbands are confined for a given amount of band bending. As the bulk doping level increases, the screening length becomes shorter, and so the potential well formed at the surface becomes narrower. This acts to increase the energy of the subband minima above the conduction band edge at the surface, leading to fewer bound subbands for a given amount of downward band bending. By control of both the surface Fermi level pinning position and the bulk doping, it is therefore possible to control the number and binding energies of the subbands within the potential well.

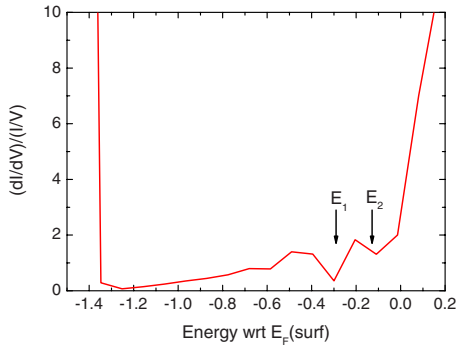

FIG. 4. (Color online) Normalized conductance from electron tunneling spectroscopy of an InN surface with a bulk carrier concentration of $n=2.5\times10^{18}$ cm^{-3} (Ref. 10). The energy is referenced to the surface Fermi level determined by Veal *et al.* (Ref. 10). The arrows show the calculated subband energy minima for a typical InN accumulation layer with this bulk carrier concentration (shown in Fig. 2).

IV. COMPARISON WITH EXPERIMENT

In this section, the results of the model calculations are compared with previous experimental observations of subband energies and dispersions at InN surfaces.

Veal *et al.*[10] have employed electron tunneling spectroscopy using a Pt-Ir tip in contact with a native oxide at the InN surface to investigate the binding energies of the subbands. Dips in the normalized conductance $(dI/dV)/(I/V)$, where I is the tunneling current and V the applied bias voltage, were attributed to tunneling into subband states. The normalized conductance for a sample with a bulk carrier concentration of $n=2.5\times10^{18}$ cm^{-3} is shown in Fig. 4.

It is of interest to compare the energy of the subbands to those calculated for a "typical" InN accumulation layer with the same bulk carrier density in Fig. 2. The energetic positions of the calculated subband minima for this accumulation layer profile are shown as vertical arrows in Fig. 4. These agree well with the subband features in the normalized conductance within the resolution of the experimental data. In order to make a more quantitative comparison, however, higher resolution experimental data would be needed. Also, perturbing effects such as tip-induced band bending[35] when a

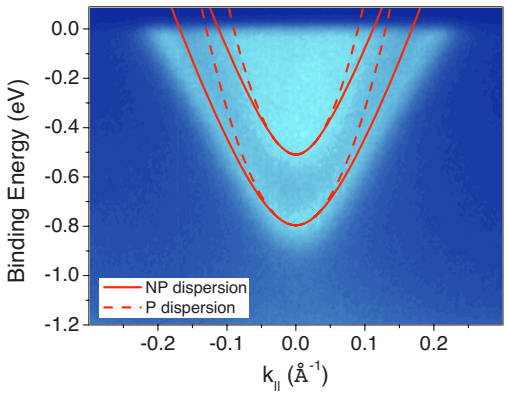

FIG. 5. (Color online) ARPES photocurrent intensity map of the parallel dispersion [along Σ ($\Gamma \rightarrow M$) in the surface plane] of two subbands in InN at 60 K (Ref. 13). Sample preparation involved two 10 min cycles of 500 eV Ar^+ ion bombardment and annealing at 300 °C. The Fermi level is at 0 eV. Simulated nonparabolic (NP) subband dispersions for InN with a surface state density of $N_{ss}=8.1\times10^{13}$ cm^{-2} and bulk density of $n_b=3.7\times10^{19}$ cm^{-3} corresponding to a downward band bending of 1.8 eV are shown (solid red line). Equivalent parabolic (P) subband dispersions are also shown (dashed red line).

bias is applied and the modification of the surface Fermi level pinning at an oxidized surface may need to be addressed.

Colakerol *et al.*[13] have investigated further the subband states at InN surfaces using high resolution ARPES. Quantized states were observed at the surface, and the in-plane dispersion of these states was determined from photocurrrent intensity maps as a function of parallel wave vector and binding energy. The photocurrent intensity map along the Σ ($\Gamma \rightarrow M$) direction for binding energies up to 1.2 eV below the Fermi level for an InN sample prepared by two 10 min cycles of 500 eV Ar^+ ion bombardment and annealing at 300 °C is shown in Fig. 5.

The two dispersions observed in the photocurrent map have been attributed to the parallel dispersion of two subbands. Simulations for InN with a surface state density of $N_{ss}=8.1\times10^{13}$ cm^{-2} and bulk density of $n_b=3.7\times10^{19}$ cm^{-3}, corresponding to a downward band bending of 1.8 eV, result in two confined subbands with their minima located 0.80 and 0.51 eV below the Fermi level at the surface, in agreement with the experimental results.

The dispersions resulting from these calculations are shown relative to the experimental dispersions in Fig. 5. At low parallel wave vector, there is good agreement between the calculated and experimental dispersions, although these diverge somewhat at higher wave vector. This may be due to small errors in the bulk conduction band edge effective mass used, failure of the Kane $\mathbf{k}\cdot\mathbf{p}$ bulk dispersion relations at higher wave vector, and neglecting the (albeit small) anisotropy of the conduction band dispersion in wurtzite InN.

Despite the slight divergence of the calculated and experimental dispersions at high parallel wave vectors, a distinct nonparabolicity is evident in both the experimental and model dispersions. The subband minimum momentum effective masses, determined from the calculated subband dispersions, are $0.080m_0$ and $0.055m_0$ for the first (E_1) and second (E_2) subbands, respectively. The equivalent parabolic dispersion for these effective masses is also shown in Fig. 5, indicating the importance of including nonparabolicity in the calculations. The effective masses determined here are somewhat smaller than those determined by Colakerol *et al.*[13] However, in their analysis, the potential well was approximated by an exponential function; such differences in the effective mass are therefore not surprising.

It should be noted that, while the surface state density required to reproduce the experimental data is within the range of previously measured experimental values,[3,29,36–38] it is somewhat higher than those typically observed at clean InN surfaces.[3,29] The reasons for this may be due to the surface preparation treatment, which involved Ar^+ ion bombardment and annealing at 300 °C. Ar^+ ion bombardment has been shown[39] to preferentially sputter N, leading to an In enrichment of the surface. This has been shown,[40] in the similar case of InAs, to lead to an increase in the near-surface carrier density; similar effects would be expected for InN, which may therefore increase the surface state density over that of a clean surface prepared without ion bombardment and annealing.

V. CONCLUSIONS

A simple method for calculating bound energies and parallel dispersion relations for subbands in surface electron accumulation layers was presented. The Poisson equation, governing the potential variation near the surface, is solved within a modified Thomas-Fermi approximation, which approximately takes account of the quantum-mechanical influence of an infinite potential barrier at the surface. The Schrödinger equation is numerically solved for the resulting one-electron potential. The effects of a nonparabolic conduction band are included for both solving the Poisson equation and the Schrödinger equation. The numerical solution of the Schrödinger equation yields nonparabolic subband dispersion relations in the plane of the surface.

The method of calculation was shown to give results very similar to full self-consistent Poisson-Schrödinger solutions of the equivalent problem for InAs surfaces. The specific case of InN was addressed in detail, due to the extreme band bending previously observed at these surfaces. Two bound states were predicted for a typical moderately doped *n*-type InN sample, with distinctly nonparabolic subband dispersions. An increase in surface state density leads to a deeper potential well at the surface which was seen to increase the number of subbands and depth at which they are bound. In contrast, increasing the bulk doping was seen to reduce the number of bound subbands as the screening length is reduced, leading to narrower potential wells at the surface.

The model calculations were compared with experimental results. Calculations for a typical InN surface were seen to be consistent with electron tunneling spectroscopy results. Additionally, model calculations of subband energies and parallel dispersions showed agreement with those observed by angle resolved photoemission spectroscopy.

ACKNOWLEDGMENTS

T. Inaoka is thanked for providing the results of his Poisson-Schrödinger calculations for InAs. M. H. Zareie, M. R. Phillips, L. Colakerol, and K. E. Smith are acknowledged for the InN electron tunneling and angle resolved photoemission spectroscopy experimental data, respectively. We also acknowledge the Engineering and Physical Sciences Research Council, U.K., for financial support under Grant No. EP/C535553/1.

*c.f.mcconville@warwick.ac.uk

[1] W. Mönch, *Electronic Properties of Semiconductor Interfaces* (Springer, Berlin, 2004).
[2] M. Noguchi, K. Hirakawa, and T. Ikoma, Phys. Rev. Lett. **66**, 2243 (1991).
[3] I. Mahboob, T. D. Veal, C. F. McConville, H. Lu, and W. J. Schaff, Phys. Rev. Lett. **92**, 036804 (2004).
[4] H. Lüth, *Surfaces and Interfaces of Solid Materials*, 3rd ed. (Springer, Berlin, 1998), p. 376.
[5] A. B. Fowler, F. F. Fang, W. E. Howard, and P. J. Stiles, Phys. Rev. Lett. **16**, 901 (1966).
[6] A. Kamgar, P. Kneschaurek, G. Dorda, and J. F. Koch, Phys. Rev. Lett. **32**, 1251 (1974).
[7] D. C. Tsui, Phys. Rev. Lett. **24**, 303 (1970).
[8] D. C. Tsui, Phys. Rev. B **4**, 4438 (1971).
[9] D. C. Tsui, Phys. Rev. B **8**, 2657 (1973).
[10] T. D. Veal, L. F. J. Piper, M. R. Phillips, M. H. Zareie, H. Lu, W. J. Schaff, and C. F. McConville, Phys. Status Solidi A **204**, 536 (2007).
[11] T. D. Veal, L. F. J. Piper, M. R. Phillips, M. H. Zareie, H. Lu, W. J. Schaff, and C. F. McConville, Phys. Status Solidi A **203**, 85 (2006).
[12] V. Y. Aristov, G. Le Lay, V. M. Zhilin, G. Indlekofer, C. Grupp, A. Taleb-Ibrahimi, and P. Soukiassian, Phys. Rev. B **60**, 7752 (1999).
[13] L. Colakerol, T. D. Veal, H.-K. Jeong, L. Plucinski, A. DeMasi, T. Learmonth, P.-A. Glans, S. Wang, Y. Zhang, L. F. J. Piper, P. H. Jefferson, A. Fedorov, T.-C. Chen, T. D. Moustakas, C. F. McConville, and K. E. Smith, Phys. Rev. Lett. **97**, 237601 (2006).
[14] G. A. Baraff and J. A. Appelbaum, Phys. Rev. B **5**, 475 (1972).
[15] D. H. Ehlers and D. L. Mills, Phys. Rev. B **34**, 3939 (1986).
[16] S. R. Streight and D. L. Mills, Phys. Rev. B **37**, 965 (1988).
[17] T. Inaoka, Surf. Sci. **431**, 156 (1999).
[18] S. Abe, T. Inaoka, and M. Hasegawa, Phys. Rev. B **66**, 205309 (2002).
[19] G. Paasch and H. Übensee, Phys. Status Solidi B **113**, 165 (1982).
[20] J.-P. Zöllner, H. Übensee, G. Paasch, T. Fiedler, and G. Gobsch, Phys. Status Solidi B **134**, 837 (1986).
[21] H. Übensee, G. Paasch, and J.-P. Zöllner, Phys. Rev. B **39**, 1955 (1989).
[22] E. O. Kane, J. Phys. Chem. Solids **1**, 249 (1957).
[23] R. Goldhahn *et al.*, Phys. Status Solidi A **203**, 42 (2006).
[24] T. Hofmann, T. Chavdarov, V. Darakchieva, H. Lu, W. J. Schaff, and M. Schubert, Phys. Status Solidi C **3**, 1854 (2006).
[25] W. Mönch, *Semiconductor Surfaces and Interfaces* (Springer, Berlin, 2001).
[26] J. M. Ziman, *Principles of the Theory of Solids* (Cambridge University Press, Cambridge, 1972).
[27] J. Wu, W. Walukiewicz, W. Shan, K. M. Yu, J. W. Ager III, S. X. Li, E. E. Haller, H. Lu, and W. J. Schaff, J. Appl. Phys. **94**, 4457 (2003).
[28] B. R. Nag, Phys. Status Solidi B **237**, R1 (2003).
[29] P. D. C. King, T. D. Veal, C. F. McConville, F. Fuchs, J. Furthmüller, F. Bechstedt, P. Schley, R. Goldhahn, J. Schörmann, D. J. As, K. Lischka, D. Muto, H. Naoi, Y. Nanishi, Hai Lu, and W. J. Schaff, Appl. Phys. Lett. **91**, 092101 (2007).
[30] I. Mahboob, T. D. Veal, L. F. J. Piper, C. F. McConville, H. Lu, W. J. Schaff, J. Furthmüller, and F. Bechstedt, Phys. Rev. B **69**, 201307(R) (2004).
[31] P. D. C. King, T. D. Veal, P. H. Jefferson, S. A. Hatfield, L. F. J. Piper, C. F. McConville, F. Fuchs, J. Furthmüller, F. Bechstedt, H. Lu, and W. J. Schaff, Phys. Rev. B **77**, 045316 (2008).
[32] H. Lu, W. J. Schaff, and L. F. Eastman, J. Appl. Phys. **96**, 3577 (2004).
[33] V. Lebedev *et al.*, J. Appl. Phys. **101**, 123705 (2007).
[34] V. Y. Aristov, G. L. Lay, P. Soukiassian, K. Hricovini, J. E. Bonnet, J. Osvald, and O. Olsson, J. Vac. Sci. Technol. B **12**, 2709 (1994).
[35] R. M. Feenstra, Phys. Rev. B **50**, 4561 (1994).
[36] H. Lu, W. J. Schaff, L. F. Eastman, and C. E. Stutz, Appl. Phys. Lett. **82**, 1736 (2003).
[37] C. H. Swartz, R. P. Tompkins, N. C. Giles, T. H. Myers, H. Lu, W. J. Schaff, and L. F. Eastman, J. Cryst. Growth **269**, 29 (2004).
[38] T. B. Fehlberg, G. A. Umana-Membreno, C. S. Gallinat, G. Koblmüller, S. Bernardis, B. D. Nener, G. Parish, and J. S. Speck, Phys. Status Solidi C **4**, 2423 (2007).
[39] S. Krischok *et al.*, Surf. Sci. **566-568**, 849 (2004).
[40] G. Bell, C. McConville, and T. Jones, Appl. Surf. Sci. **104-105**, 17 (1996).